Title

A two-step strategy for delivering particles to targets hidden within microfabricated porous media

Journal

Science Advances, 7(33)

ISSN

2375-2548

Authors

Tan, Huanshu
Banerjee, Anirudha
Shi, Nan
et al.

Publication Date

2021-08-13

DOI

10.1126/sciadv.abh0638

Peer reviewed

APPLIED PHYSICS

A two-step strategy for delivering particles to targets hidden within microfabricated porous media

Huanshu Tan[1]*†, Anirudha Banerjee[1‡], Nan Shi[2], Xiaoyu Tang[1§], Amr Abdel-Fattah[2], Todd M. Squires[1]*

The delivery of small particles into porous environments remains highly challenging because of the low permeability to the fluids that carry these colloids. Even more challenging is that the specific location of targets in the porous environment usually is not known and cannot be determined from the outside. Here, we demonstrate a two-step strategy to deliver suspended colloids to targets that are "hidden" within closed porous media. The first step serves to automatically convert any hidden targets into soluto-inertial "beacons," capable of sustaining long-lived solute outfluxes. The second step introduces the deliverable objects, which are designed to autonomously migrate against the solute fluxes emitted by the targets, thereby following chemical trails that lead to the target. Experimental and theoretical demonstrations of the strategy lay out the design elements required for the solute and the deliverable objects, suggesting routes to delivering colloidal objects to hidden targets in various environments and technologies.

INTRODUCTION

Transporting colloidal objects to specific locations within porous media is essential for many applications, including drug or cargo delivery (*1*–*3*), material fabrication (*4*, *5*), oil discovery and recovery (*6*, *7*), chemical and biochemical sensing (*8*, *9*), and remediation of polluted soils and groundwater aquifers (*10*–*12*). The delivery of small particles into porous environments remains highly challenging due to the low permeability to the fluids that carry these colloids (*13*). Although suspended colloidal objects can explore porous media via Brownian motion, this stochastic process is often impractically slow: Particles with diffusivity D require a time $\tau_D \sim L^2/D$ to diffuse a distance L, meaning that micrometer-diameter particles require nearly 1 month to migrate just 1 mm by diffusion in water. Alternative mechanisms have thus been explored to drive particle migration using nonequilibrium gradients, e.g., surface tension gradients (Marangoni) (*14*, *15*), diffusiophoresis (*16*), electrophoresis (*17*), and chemotaxis (*18*). Nonequilibrium fluxes have been imposed using gradients of various salts (*19*–*21*), surfactants (*22*, *23*), polymers (*24*), and enzyme substrates (*25*) or of field variables like temperature (*26*), pH (*27*, *28*), or dissolved gas (*29*). A variety of particle types have been driven in this way, including solid particles, droplets, or bubbles (*30*–*32*), enzymes (*25*), and cells (*33*). Although particle delivery by such means is indeed faster than by diffusion alone, the migration nonetheless occurs in a manner insensitive to the location (or even presence) of their intended targets.

In a variety of medical, energy, environmental, and technological applications, it would be advantageous to deliver particles or droplets to specific targets within porous media. Even if the locations of such targets were known, it would be extremely challenging, or even impossible, to deliver particles specifically to them. Further compounding this challenge in most practical situations is the fact that targets are generally hidden within the media.

Here, we demonstrate a strategy to cause suspended objects to autonomously migrate toward targets hidden within porous media. Our strategy builds upon nonequilibrium "soluto-inertial interactions" between "beacons" that slowly release some solute over long distance and time scales and suspended colloids that migrate diffusiophoretically in response to the solute flux (*22*, *34*). In heat transfer, objects with high heat capacity surrounded by poor heat transfer media are said to have large thermal inertia because they react slowly to changes in ambient temperature. By analogy, high–solute capacity objects that are immersed in poor mass transfer environments have strong soluto-inertia and slowly absorb or release solute in response to changes in the surrounding solution.

In the first step of the two-step strategy, the porous media are exposed to a solute that naturally concentrates within any targets located within the media. Hidden targets are thereby converted into soluto-inertial beacons that emit long-ranged and long-lasting chemical outfluxes when the externally imposed solute is removed. In the second step, suspended colloidal objects migrate along these chemical outfluxes, which are automatically directed specifically to the desired targets.

RESULTS

Two-step strategy for target-delivering particles and experimental verification

Figure 1 illustrates the two-step strategy using a simple model geometry: a main channel, along which fluid may flow, that branches off to a micropore containing a "target" at its dead end (Fig. 1A). The first step (Fig. 1, B and C) is a solute-loading step, in which target-favorable solute is flowed along the main channel and diffuses into micropore toward the target (Fig. 1B), ultimately reaching an equilibrium where the solute is concentrated within the target (Fig. 1C). The particle delivery step then follows (Fig. 1, D and E).

[1]Department of Chemical Engineering, University of California, Santa Barbara, Santa Barbara, CA 93106-5080, USA. [2]Saudi Aramco, EXPEC Advanced Research Center, Dhahran 31311, Saudi Arabia.
*Corresponding author. Email: huanshutan@gmail.com (H.T.); squires@engineering.ucsb.edu (T.M.S.)
†Present address: Center for Complex Flows and Soft Matter Research and Department of Mechanics and Aerospace Engineering, Southern University of Science and Technology, Shenzhen 518055, P.R. China.
‡Present address: Performance Silicones Research and Development, The Dow Chemical Company, 2200 West Salzburg Road, Auburn, MI 48611, USA.
§Present address: Mechanical and Industrial Engineering, Northeastern University, 360 Huntington Avenue, Boston, MA 02115, USA.

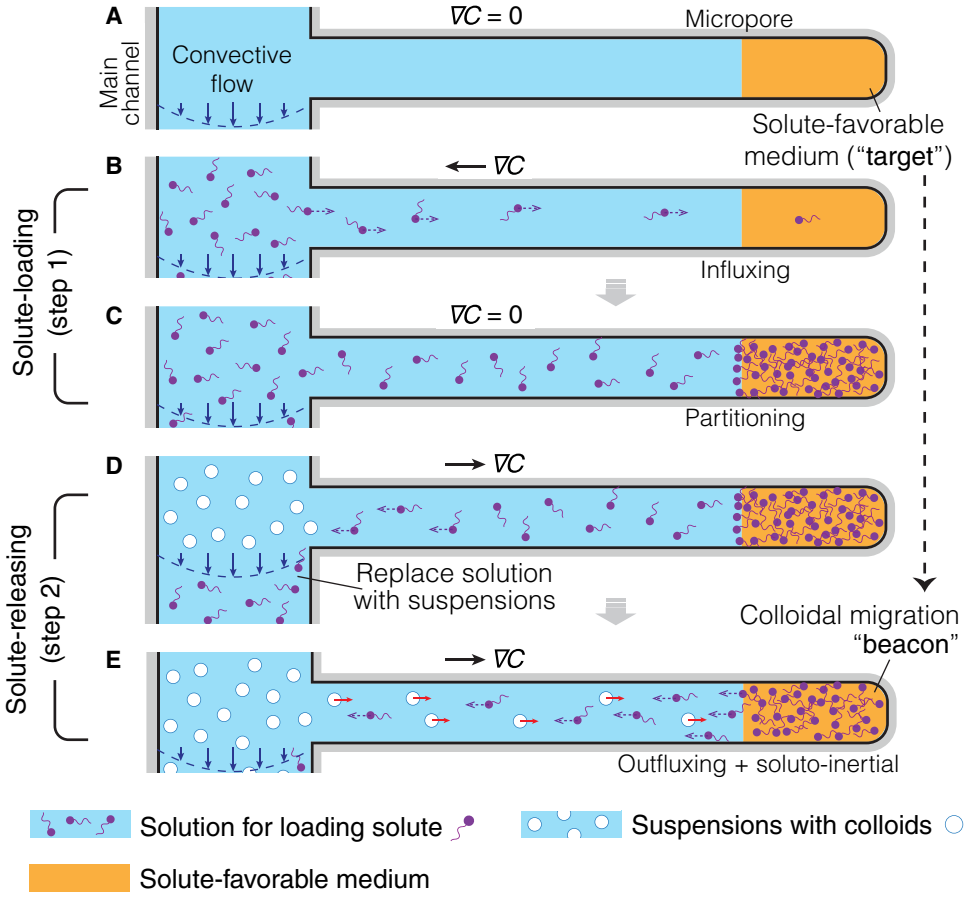

Fig. 1. Two-step strategy for targeted colloidal delivery. (**A**) A micropore branches off from the main channel, which can carry a convective flow. A solute-favorable medium (target) is placed at the end of the micropore, where it is initially in an equilibrium state. (**B**) In the first (loading) step, solution is flowed continuously along the main channel to drive a diffusive influx of solute toward the target until (**C**) reaching a new equilibrium with a solute-saturated target in the micropore. (**D**) In the second (delivery) step, a colloidal suspension is flowed in the main channel, replacing the loading solution, thereby triggering solute outflux from the micropore. (**E**) The solute outflux is maintained by the solute-saturated target and drives to a sustained colloidal migration toward the target. The solute-saturated target is converted to a soluto-inertial "beacon," emitting solute and thus attracting colloidal migration.

In this second step, the colloidal suspension is flowed through the main channel, removing the solute at the mouth of the micropore and initiating a diffusive outflux of solute that is sustained by the soluto-inertial target (Fig. 1D). The suspended particles then migrate up this solute gradient—e.g., by soluto-capillary or diffusiophoresis—naturally following the chemical flux to ultimately reach the target (Fig. 1E).

We demonstrate this two-step strategy with microfluidic devices with a simple T design—a main channel (width, 450 μm; height, 20 μm) connected to a straight subchannel acting as a micropore (length, $L = 1500$ μm; width, 150 μm; height, 20 μm), as illustrated in Fig. 2A. A polyethelene glycol diacrylate (PEG-DA) target (length, $L_T = 300$ μm) was photopolymerized at the end of the micropore. Initially, the entire channel system was filled with water (see the Supplementary Materials). During the target-loading step, a 600 mM butanol solution, under its solubility of 850 mM, was flowed through the main pore before switching the flow in the main channel from the butanol solution to a suspension of silicon oil drops (mean radius, 2.2 μm; SD, 0.8 μm) and initiating the particle delivery step. Butanol diffuses out of the micropore and is convected away by the main channel flow; the butanol flux is maintained by the soluto-inertial release from the PEG-DA target. The silicon oil drops migrate up butanol gradients toward the target (movie S1), as surface tension gradients along the drop surface drive soluto-capillary flows: The drop interface is pulled from the pole with highest butanol concentration (and therefore lowest surface tension) toward the opposite pole, dragging fluid with it, which causes the drop to move (*14*, *15*). Droplet path lines with colors coded by time in Fig. 2B show clear, directed migration toward the target, during the first 10 min (left) and even after 3 hours (right).

Figure 2 (C to E) shows control experiments that verify the two-step strategy works as intended. For example, solute loaded into a micropore requires some time to unload, even if that micropore contains no target to sustain the solute outflux. One would then expect particles to migrate into the empty micropore, against the solute flux, during the conventional diffusion time scale but not over the longer soluto-inertial time scale. Figure 2C confirms this expectation—after an "empty" micropore is loaded with a solute-loading step, droplets initially migrate into the micropore but stop long before reaching the end of the micropore (movie S2). This stands in contrast with Fig. 2B, where the loaded target sustains the butanol gradient over the much longer soluto-inertial time, continually attracting droplets

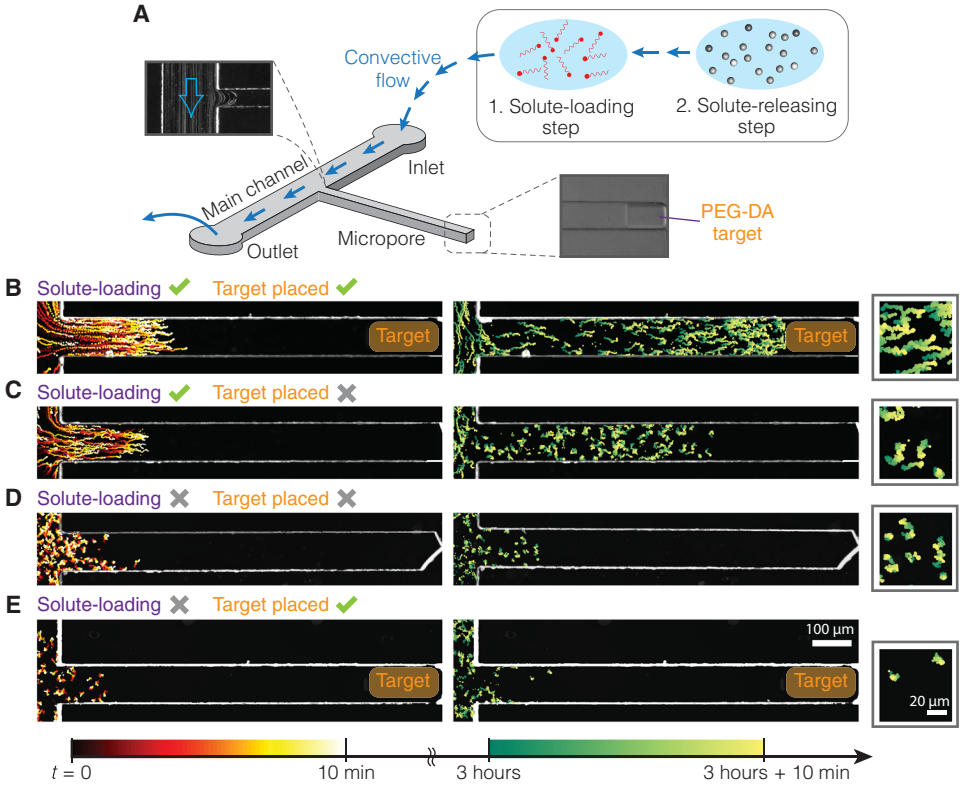

Fig. 2. Enhanced and prolonged colloidal migration toward a target. (**A**) Polyethelene glycol diacrylate (PEG-DA) target is photopolymerized within a micropore to demonstrate the two-step targeted delivery strategy. Colloidal path lines along the main channel confirm no convective delivery along the micropore. (**B** to **E**) Chronophotographic pictures of silicone oil droplets (mean radius, 2.2 μm; SD, 0.8 μm), color-coded by time, display their locomotion during 10-min intervals: (left) immediately after the start of the delivery step and (right) following 3 hours of particle delivery. (B) The full two-step delivery system (a 3-hour solute-loading step with 600 mM butanol solution) drives sustained colloidal motion toward the target even after 3 hours (movie S1). (C) Particles initially migrate into a target-free pore preloaded with 600 mM butanol solution. However, droplets stop well before reaching the end of the pore, and so no directed motion after 3 hours (movie S2) (D) occurs. With neither target nor preloading, colloids simply diffuse around the pore mouth. (E) Nonloaded targets do not attract colloidal migration (movie S3). In the last column, the zoom-in images at 3 hours highlight the enhanced and prolonged colloidal locomotions in case (B).

even after several hours. To confirm that the initial delivery of particles into the empty micropore is driven by the transient outflux of solute, Fig. 2D shows the particle delivery step without any solute-loading step. Brownian motion, rather than directed migration, is observed. Last, a third control experiment tests the possibility that the target itself might leach out some solute that drives the colloidal migration, rather than the butanol that was intentionally preloaded during the first step. Figure 2E excludes that possibility, showing a micropore that contains a target, for which no solute-loading step was applied; instead, only droplet suspension was flowed along the main channel. The fact that only Brownian motion is observed (movie S3), confirms that solute must be loaded for directed delivery of particles.

Theoretical foundation

Having experimentally demonstrated the two-step strategy, we now develop a theoretical framework for its quantitative understanding. We analyze a model geometry (Fig. 3A) based on the experiments of Fig. 2 and focus specifically on a micropore of total length L, containing a target of length $L_T = 0.1L$ at the end of a pore of length $L_S = 0.9L$. Solute concentration C_S diffuses with diffusivity D_S along the pore, obeying the one-dimensional diffusion equation $\dot{C}_S = D_S C_S''$ between $0 \le x \le L_S$, and target solute C_T to diffuse with diffusivity D_T within the target, between $L_S \le x \le L$. At the solution/target boundary ($x = L_S$), solute fluxes must balance ($D_S C_S' = D_T C_T'$), and solution and target concentrations obey contact equilibrium—here assumed via a partition coefficient $C_T = PC_S$. A no-flux boundary condition $C'(L) = 0$ prevents solute from leaving the dead end of the micropore. The pore is initially devoid of solute, and then solute-loading step is initiated when the concentration at the micropore mouth is raised to loading concentration C_S^e.

Figure 3A (movie S4) shows finite-difference calculations of the solute concentrations under mild partitioning ($P = 3$), showing solute approaching steady state $C_T = 3C_S$ over a time scale approximately three times longer than the time scale L^2/D_S for solute to diffuse through an empty micropore, as discussed below. Likewise, the particle delivery step, initiated by removing solute at the micropore mouth [$C_S(0, t) = 0$], shows a solute outflux from the target that is sustained for a comparable time (movie S5).

The solute absorbed by the target and the time required to do so both increase in direct proportion to the partition coefficient P, shown in Fig. 3B, with analogous results for the particle delivery (target releasing) step. The solute concentration gradient, which is responsible for driving particle migration, also persists over a time scale proportional to P, as evident from Fig. 3C.

These qualitative and quantitative features can be captured by a simple scaling argument. The computations in Fig. 3 reveal the shape

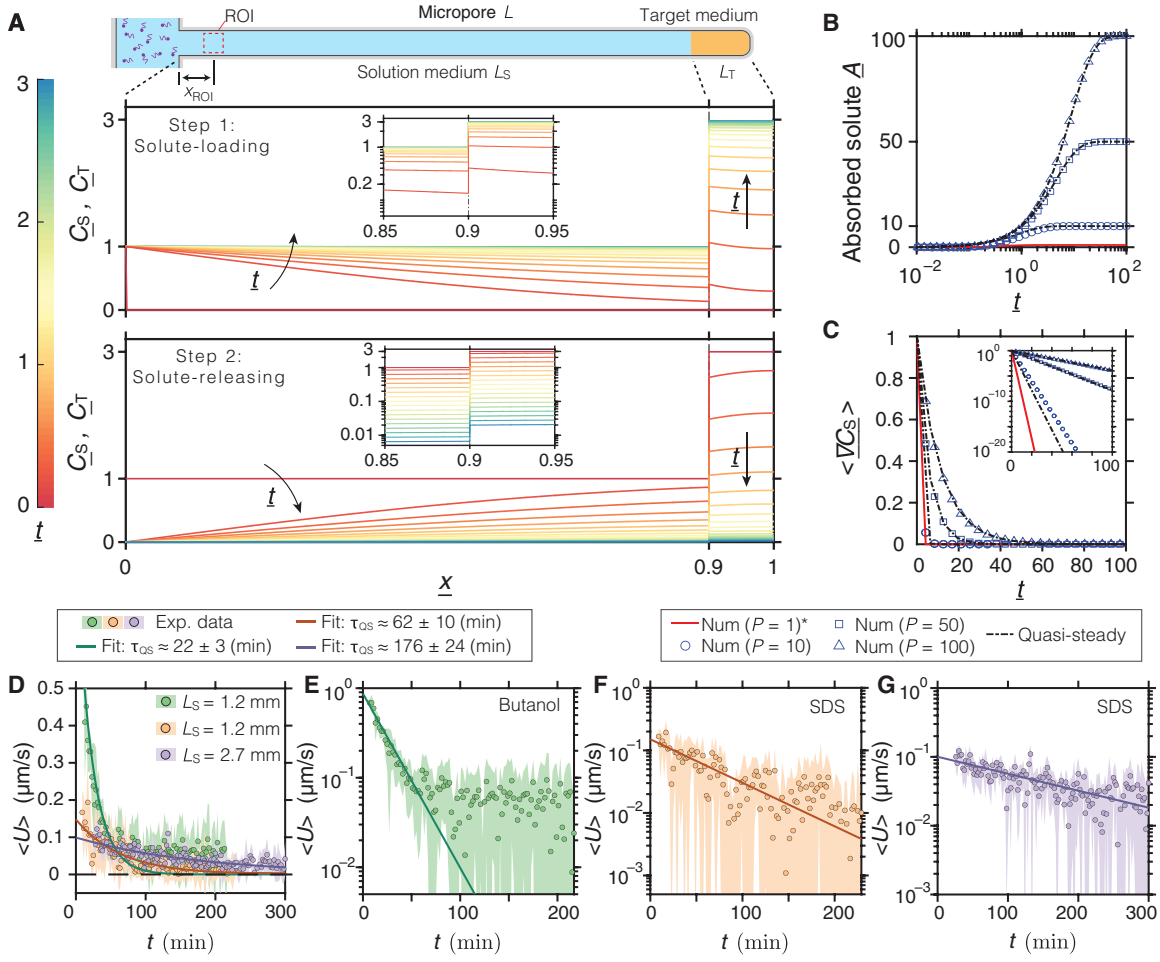

Fig. 3. Diffusion dynamics of the two-step strategy. (**A**) Simulation of the diffusion process in the micropore shows the evolution of concentration field both in the solution and target media (movies S4 and S5). The target-to-micropore length ratio is 0.1, and the target-to-solution partition constant P is 3 (see the Supplementary Materials). Underlines indicate nondimensional variables. C_S and C_T are scaled by the loading solution concentration C_S^e, x by the micropore length L, and t by the diffusion time scale L^2/D_S. ROI, region of interest. (**B**) In the solute-loading step, the total absorbed solute $A \coloneqq \int_{L_T} C_T dx$, scaled by $\int_{L_T} C_S^e dx$, grows with partition constant P, as does the loading time. (**C**) During the solute-releasing step, the mean solute concentration gradient $\langle \nabla C_S \rangle$, scaled by C_S^e/L_S, persists longer as P increases. The inset is in a log-linear space. Dashed lines represent the quasi-steady approximation (Eq. 2). (**D**) Experiments show the exponential decay of the colloidal migration speed averaged over the ROI in (A). (**E** to **G**) Datasets in a log-linear space separately. The green data: Butanol is solute and L_S = 1.2 mm, L_T = 300 μm, x_{ROI} = 110 μm. The orange data: SDS is solute and L_S = 1.2 mm, L_T = 300 μm, x_{ROI} = 110 μm. The purple data: SDS is solute and L_S = 2.7 mm, L_T = 300 μm, x_{ROI} = 360 μm. Solid lines represent fits to $U = U_0 e^{-t/\tau_{QS}}$ and the quasi-steady approximation. Error bars represent SDs (fitting details refer to see the Supplementary Materials).

of the concentration profiles to remain approximately linear in the micropore and approximately constant in the target (Fig. 3A), even as the magnitudes of these profiles grow or decrease. Such behavior motivates a quasi-steady approximation to the fully transient diffusive processes in the two media. The solute concentration in the micropore is approximated with a uniform gradient $C_S = C_S^e + (C_S^i(t) - C_S^e)\,x/L_S$, where $C_S^i(t)$ is the solution concentration at the solution/target interface, and the target concentration $C_T(t)$ is approximated as spatially uniform, but time dependent. The diffusive flux into the target, given by

$$j \sim D_S \frac{\Delta C_S}{\Delta x} \sim D_S \frac{C_S^i(t) - C_S^e}{L_S} \tag{1}$$

changes the concentration in the target, via

$$L_T \frac{dC_T}{dt} = D_S \frac{C_S^e - C_S^i}{L_S} = D_S \frac{P C_S^e - C_T}{P L_S} \tag{2}$$

The latter step relates the two unknown quantities, $C_S^i(t)$ and $C_T(t)$, by the partition coefficient P. Quasi-steady solutions to (Eq. 2) are

$$C_T(t) = P C_S^e (1 - e^{-t/\tau_{QS}}) \text{ loading} \tag{3}$$

$$C_T(t) = P C_S^e e^{-t/\tau_{QS}} \text{ unloading} \tag{4}$$

where

$$\tau_{QS} = \frac{P L_S L_T}{D_S} \tag{5}$$

is the time scale for the target to absorb or release solute.

The quasi-steady approach is based on two basic assumptions. First, the assumed uniformity of the target concentration requires that the time scale $\tau_T \sim L_T^2/D_T$ for the target concentration to reach quasi-steady state is much faster than for the solute in the micropore,

$\tau_S \sim L_S^2/D_S$—constraining the target to be small enough ($L_S \gg L_T\sqrt{D_S/D_T}$). Second, the concentration profile within the micropore must reach a quasi-steady state much more quickly than the quasi-steady time scale τ_{QS}, which constrains the partition coefficient to be large enough: $P \gg L_S/L_T$. Dashed lines in Fig. 3 (B and C) compare the quasi-steady expression (Eq. 2) with numerical computations for $L_S/L_T = 9$, revealing excellent agreement when $P \gg 9$, moderate agreement when $P \sim 9$, and poor agreement when $P = 1$.

The discussion to this point has focused on the behavior of the solute: The first step loads the target with solute and effectively converts it into a soluto-inertial beacon. During the particle delivery step, the solute-loaded target sustains a solute outflux directed from the target toward the mouth of the micropore. The delivery process requires particles to migrate up solute gradients against the solute outflux maintained by the target. Suspended particles, molecules, and droplets are known to migrate in response to solute gradients through various mechanisms, including diffusiophoresis (*14*, *16*, *35*–*37*), thermophoresis (*38*), thermocapillary (*31*), and soluto-capillary migration (*15*, *39*). The present experiments deliver silicon oil drops to targets using soluto-capillary migration: The solute is surface active on the oil/water interface, so that solute gradients cause surface tension gradients along the droplet surface, driving a surface flow along the droplet that propels it up the surfactant gradient. Theories for soluto-capillary migration (*15*, *39*, *40*) generally predict droplet migration speed to be proportional to the solute gradient via $U = D_M \nabla C_S$, where D_M is the soluto-capillary mobility of the droplet.

Particle delivery velocities U are expected to decay over time in the same way that the solute gradients do. Quasi-steady arguments (Eq. 4) predict the gradient $\nabla C_S \sim C_T(t)/L_S$ (and therefore the droplet migration velocity) to decay exponentially over τ_{QS} (Eq. 5).

Experiments verify the exponential decay of migrating speed, as demonstrated in Fig. 3D. In particular, a PEG-DA target at the dead end of a pore emits a solute (butanol) that had been loaded during the first step; this butanol flux attracts silicon oil droplets from the main channel whose speed decays exponentially with a measured time $\tau_{QS} = 22 \pm 3$ min (green data). The two-step strategy is not limited to butanol: The purple and orange datasets show droplet migration velocities driven by gradients of the anionic surfactant SDS, which loads into the PEG-DA target medium (*22*, *41*) and is surface active at the water–silicon oil interface (*42*). SDS was loaded at a concentration $C_S^e = 7.5$ mm under the critical micelle concentration. The orange dataset, with velocity decay time $\tau_{QS} = 62 \pm 10$ min, was taken in the standard micropore geometry ($L_S = 1.2$ mm, $L_T = 300$ μm), whereas the purple dataset ($\tau_{QS} = 176 \pm 24$min) was measured in a longer channel ($L_S = 2.7$ mm, $L_T = 300$ μm). The quasi-steady time scale (Eq. 5) predicts the velocity decay time scale in these two geometries to differ by a factor $2.7/1.2 \approx 2.25$, which compares favorably with the measured ratio $176/62 \approx 2.84$, further confirming the mechanism that we have outlined for the two-step strategy.

Targeted transport in a branch network

Last, we turn to more complicated porous geometries to demonstrate that the two-step strategy specifically and rapidly delivers particles to hidden targets. Particularly, Fig. 4 replaces the simple, straight micropore of Fig. 2 with a hierarchically branched micropore network, i.e., a microfabricated porous media. Particles driven into this pore are faced with multiple equivalent paths, only one of which leads to the target. Six identical dead ends terminate the model pore: PEG-DA target is placed in one, a decane "antitarget" [for which the butanol partition coefficient $P \approx 0.16$ (*43*)] is placed in another, and the remaining four are left empty. Notably, the 3.3-mm distance between the main channel and the target implies that 1-μm particles would require more than 8 months reaching the target by diffusion alone!

We implemented the two-step procedure with the same material system as shown in Fig. 2B: butanol as the solute, PEG-DA as the target, and silicon oil droplets as the deliverable. The solute-loading time is estimated to be approximately 24 hours from the simulation (see the Supplementary Materials), so the solute-loading step was maintained for 32 hours, after which the particle-loading step was initiated.

Figure 4A shows chronophotographic images of the colloidal droplet migration during three different quarter hours: the first 15 min of the particle delivery step (left), after 5 hours (middle), and after 10 hours (right) (refer to movie S6). Droplets migrate more than 1 mm during the first 15 min of the delivery step—but not far enough to reach the first branch. After 5 hours, by contrast, droplets have not only reached the target but are overwhelmingly making the correct "choices" to reach the target. Particles continue to migrate toward the target even after 10 hours. Those few droplets that make the "wrong" choice at the first branch (due to the initial transient outflux, analogous to Fig. 2C) ultimately exhibit simple Brownian motion, rather than any directed migration. Droplets are driven only toward the hidden target—not toward the antitarget nor toward the empty dead ends.

Numerical computations of diffusive solute dynamics in an analogous branched network (Fig. 4B and movies S7 to S9) provide additional insight into the experimental results. Computational details can be found in the Supplementary Materials; in particular, the partition coefficient for the target $P = 10$ was chosen just for illustrative purpose. Figure 4C shows concentration fields after 10 hours (note different scales for the solution, target, and antitarget). Arrows indicate the route with the highest solute gradient, which is taken by the colloids in the experiments (Fig. 4A). Normalized solute distributions along different branches are compared in Fig. 4 (D and E): The steep rise in solute concentration in secondary branch C_{12}, compared to C_{11}, is responsible for the preferential migration around C_{12}, whereas the slight gradient along C_{11} does attract some particles. The difference is starker among tertiary branches: The branch C_{123} leading to the target has the strongest solute gradient, whereas minimal solute gradients persist in the other tertiary branches, whether leading to the antitarget (C_{113}) or to an empty dead end. The concentration in branches C_{121} and C_{122} is set by the branch point C_{123} and is therefore uniformly higher than the other three, C_{111}, C_{112}, and C_{113}. Notably, the gradients within each of the nontarget branches are essentially identical and negligible, and the gradient within the antitarget branch is even weaker because of the reduced solute storage in the antitarget ($P = 0.16$). The relative flux of particles into each branch is set by the relative strength of the gradients in those branches, which are established within the first hour of the target-releasing step (Fig. 4F).

DISCUSSION

We have demonstrated a two-step strategy that automatically delivers colloidal particles to targets hidden within porous media. Notably, this strategy requires no knowledge of where the targets are located: In the first step, a solute is introduced from outside and simply diffuses into the porous media. Whenever that solute encounters target materials—wherever they happen to be located—thermodynamic

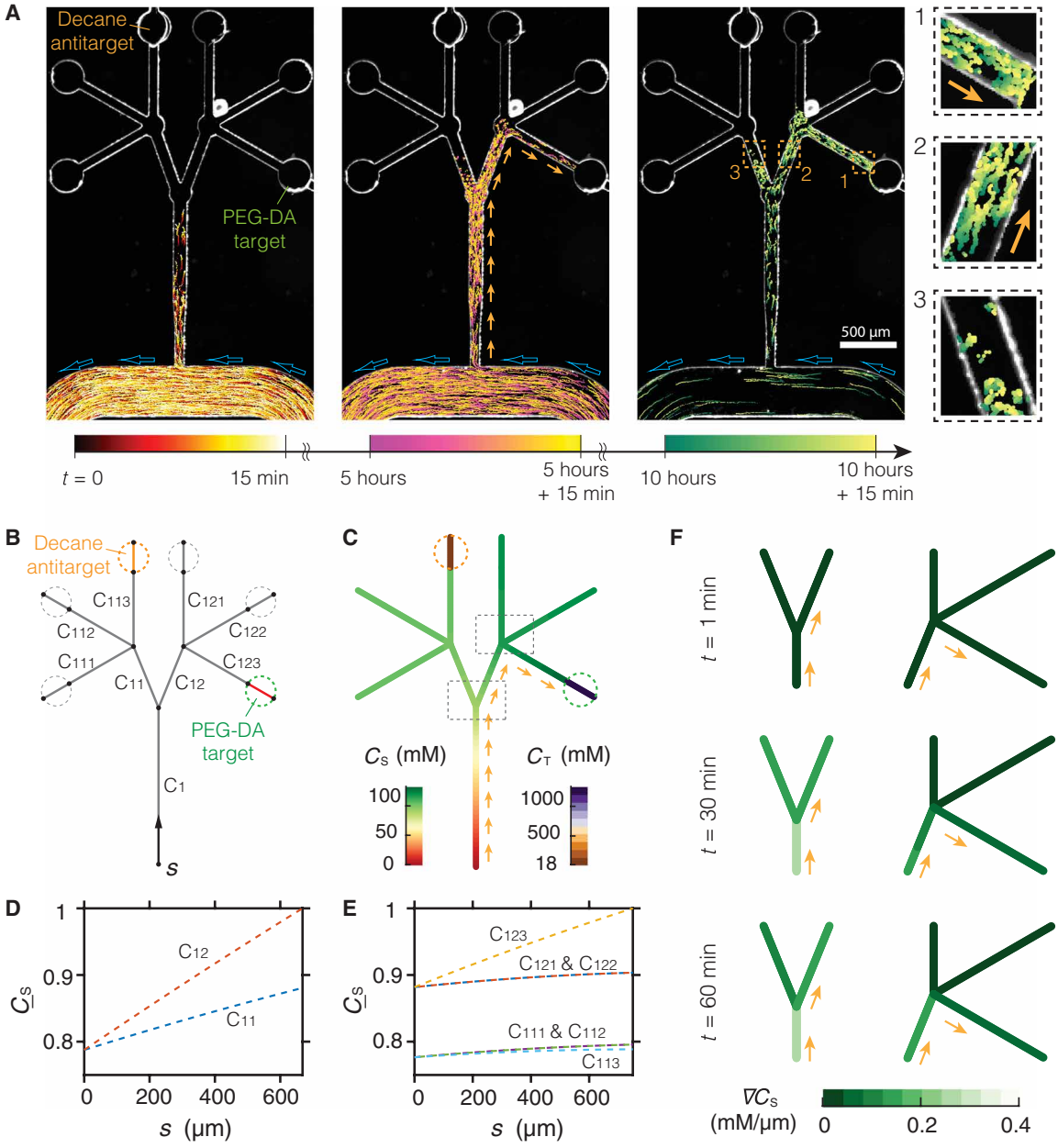

Fig. 4. Targeted delivery to a target hidden within a microchannel branching network. (**A**) A branched network consists of six identical dead-end pores, of which one contains a PEG-DA target and one contains a decane antitarget. Following a 30-hour butanol-loading step, chronophotographs of the network highlight colloidal migration during 15-min intervals following 0, 5, and 10 hours of the particle delivery step. Particles are delivered specifically to the target instead of the antitarget or empty pores (movie S6). Zoomed images highlight the persistent, directed migration after 10 hours in channels 1 and 2 on the path to the target versus Brownian motion alone in channel 3 off the target path. (**B**) Network of one-dimensional pores in a diffusion computation, where $P = 10$ for the target and $P = 0.16$ for the antitarget. (**C**) Simulated solute distribution in the network at 10 hours (movie S8). Orange arrows indicate the maximum gradient route consistent with the experimental demonstration. (**D** and **E**) Concentration comparisons among the same level segments confirm the maximum-gradient route. (**F**) Concentrations at two boxed junctions in (C) show the relative strength of the gradients in the two options, directing the colloids down the target path (movie S9).

forces drive the solute to concentrate within the target. This effectively converts the target into a soluto-inertial beacon, which initiates and maintains a long-lived solute outflux during the second step, when the loading solution is replaced with the colloidal dispersion. Not only do particles reach the targets orders of magnitude more quickly than by diffusion alone but also they are directed along paths that lead specifically to targets.

The two-step strategy requires three key elements—the target, the mediating solute, and the particles to be delivered—all of which must work together as a system. Given a target, a solute must be chosen to concentrate within the target and therefore convert it to an soluto-inertial beacon (*22*). This propensity to load into the target may occur because of a high partition coefficient (*43*), a strong adsorption or association constant, or some other basis (*22*, *44*).

Last, deliverable particles—whether droplets, colloids, solid nanoparticles or fines, cells, proteins, viruses, vesicles or capsules—must be chosen that migrate in response to these solute fluxes, e.g., via diffusiophoresis, soluto-capillary, or some other mechanism (*19*, *20*, *22*, *28*, *30*, *45*).

There is considerable flexibility in achieving the conditions required for the two-step strategy, and therefore, the design space seems quite broad for targeted delivery in various environments, applications, and technologies. The two-step strategy holds obvious advantages for applications where the target property is known, whereas its position is unknown, for example, in delivering payloads to oil trapped in tight or dead-end pores or in detecting chemical leaks (*8*, *9*).

Another possibility involves "rechargeable" materials, where targets are embedded in a porous matrix and serve as a deposit site. In this class of applications, particles [e.g., degradable polymeric microgels for drug delivery (*1*–*3*)] could be periodically introduced from the outside and delivered via the two-step strategy, thus providing a route to sustaining the potency of the loaded matrix particles. Because diffusiophoresis can drive particles up or down electrolyte gradients (*46*), depending on the relative strength and directions of the chemiphoretic and electro-diffusiophoretic contributions, it may be possible to deliver particles to targets and then to later recover them, for example, as a chemical or environmental diagnostic record.

As a third possibility, one could envision a system in which physicochemically distinct targets are embedded within a matrix, each of which prefers a different solute. In this way, particles could be driven to migrate from location to location through the serial application of distinct solvents, offering previously unidentified capabilities for nanoparticle assembly and manipulation.

The two-step strategy established and demonstrated here suggests fundamentally new capabilities for a broad spectrum of technologies. Given the variety of ways in which deliverable particles, solutes, and targets may meet the core requirements, the two-step strategy promises for fundamentally new technologies.

MATERIALS AND METHODS

Sample preparation

The silicone oil colloidal suspension was prepared by first adding 20 μl of silicone oil (20 cSt; Sigma-Aldrich) to 10 ml of deionized water and then having the solution vortexed for 20 min. The probability density function of the colloidal particle size has a normal distribution with a mean of 2.2 μm and an SD of 0.8 μm, which was calculated by imaging analyses. Stock aqueous solutions of *n*-butanol (99.4%; APC Pure) and SDS (Sigma-Aldrich) were prepared and diluted according to the experimental requirements.

Given $a \sim 10^{-6}$m–radius drops of silicon oil ($\Delta\rho \sim 10$ kg/m^3 and viscosity ratio $\lambda \sim 20$), the Stokes rise velocity $U_b \sim 2a^2\Delta\rho g/(9\mu) \sim 0.1$ μm/s and diffusivity $D \sim k_BT/(6\pi\eta_w a) \sim 1$ μm^2/s. Consequently, diffusion overwhelms gravitational rise over distances within tens of micrometers from the top of the channel. Because channels are 20 μm tall, we do not expect strong gravitational effects.

Channel fabrication

The microchannel devices used in this work were made by ultraviolet (UV)–curable epoxy (NOA 81, Norland Products). This material has excellent chemical resistance to organic solvents, is impermeable to air and water vapor, and is less prone to swelling upon contact with fluids (*47*, *48*). All the channels in this work are 20 μm thick.

We designed microchannels with AutoCAD software. The design sketch is given in the Supplementary Materials. Photomasks were printed into a high-resolution emulsion film (20,000 dots per inch; CAD/Art Services Inc.). We performed standard soft lithography procedures with the photomasks in a cleanroom environment. We spin-coated a Si wafer with a negative photoresist (SU-8). A UV light exposure through a photomask and a subsequent chemical development produced a SU-8 master wafer, where the microstructures were down. We then performed a hydrophobic coating on the master wafer with 1*H*,1*H*,2*H*,2*H*-perfluorododecyltrichlorosilane (>97%; Sigma-Aldrich) to increase its lifetime. In the next polymer molding step, we used the SU-8 master wafer to cast the microstructure into PDMS (polydimethylsiloxane; Sylgard 184; Dow Corning). We degassed the sample for 1 hour and then cured the sample at 80°C for 6 hours. Then, we peeled the cured PDMS off the wafer and produced a PDMS master wafer, where the microstructures were up. In the last step, we applied the microfluidic sticker technique (*47*, *48*) to cast the microstructure from the PDMS master wafer into UV-curable epoxy (NOA81, Norland Products). A glass cover slide (25 mm by 75 mm; Thermo Fisher Scientific) was used to seal the device with holes drilled to provide access for inlet and outlet tubing. A PDMS holder was ozone-bonded to the cover slide to provide support for inlet and outlet pins and tubings. The device was then baked at 80°C for at least 6 hours to strengthen bonding.

To have an artificial micropore with a PEG-DA target placed within, we have developed an approach by integrating the technique of UV polymerization of hydrogels in situ (*49*). We have developed a different method to artificially place a decane (≥99%; Sigma-Aldrich) target within a branching microchannel network filled with water. A description of the procedure is in the Supplementary Materials.

Experimental setup and methods

Experiments were performed using an inverted microscope (TE2000U; Nikon), and different objectives were used as required. A monochrome camera (MQ013MG-ON; Ximea) was attached to the microscope to record the experiments. To avoid contaminants in the experiment, we used the dark-field technique, instead of the fluorescent technique, to observe the colloids in the channel. A programmable syringe pump (NE-1000; New Era) was used to control the flow rate of the solution in the main channel. All the experiments were performed at room temperature around 22°C without a specific control. A optical calibration target was first used to calibrate the microscope and camera. Then, we fixed the device on the microscope stage and moved the microscope slide around to have both the micropore and a reference structure in the field of view. Then, we used the syringe pump to flow the solution of butanol or SDS though the main channel at a flow rate of 0.03 μl/min for the first target-loading step. To have the fluid system reaching a new equilibrium state, we set the loading time according to a simulation calculation (≈3 hours for a 1.5-mm-deep micropore device). After that, we started the recording with the camera first and then changed the pumping fluids to the colloidal suspension. The flow rate was also set to 0.03 μl/min.

To measure migration speeds, we recorded the colloidal migration at a fixed region of interest and performed both micro-Particle Image Velocimetry (micro-PIV) and Particle Tracking Velocimetry (PTV) calculation with the recorded images. We used a custom MATLAB code to analysis the data. A description of the procedure is in the Supplementary Materials.

Simulation methods

We assume that the diffusion process in the two steps is a one-dimensional two-medium dilute diffusion problem. We use finite-difference methods to solve the defined problem. To simulate the diffusion dynamics in a branching microchannel network, we consider the mass conservation at each branch intersection and solve the concentration field within each segment as a one-dimensional diffusion process problem. A description of the simulation implementation and the corresponding parameters are in the Supplementary Materials.

SUPPLEMENTARY MATERIALS

Supplementary material for this article is available at http://advances.sciencemag.org/cgi/content/full/7/33/eabh0638/DC1

REFERENCES AND NOTES

1. K. A. Janes, P. Calvo, M. Alonso, Polysaccharide colloidal particles as delivery systems for macromolecules. *Adv. Drug Deliv. Rev.* **47**, 83–97 (2001).
2. D. Patra, S. Sengupta, W. Duan, H. Zhang, R. Pavlick, A. Sen, Intelligent, self-powered, drug delivery systems. *Nanoscale* **5**, 1273–1283 (2013).
3. Y. Yang, M. A. Bevan, Cargo capture and transport by colloidal swarms. *Sci. Adv.* **6**, eaay7679 (2020).
4. O. D. Velev, A. M. Lenhoff, Colloidal crystals as templates for porous materials. *Curr. Opin. Colloid Interface Sci.* **5**, 56–63 (2000).
5. G. Cao, *Nanostructures and Nanomaterials: Synthesis, Properties and Applications* (World Scientific, 2004).
6. K. Guo, H. Li, Z. Yu, In-situ heavy and extra-heavy oil recovery: A review. *Fuel* **185**, 886–902 (2016).
7. A. Perazzo, G. Tomaiuolo, V. Preziosi, S. Guido, Emulsions in porous media: From single droplet behavior to applications for oil recovery. *Adv. Colloid Interface Sci.* **256**, 305–325 (2018).
8. B. Ezhilan, W. Gao, A. Pei, I. Rozen, R. Dong, B. Jurado-Sanchez, J. Wang, D. Saintillan, Motion-based threat detection using microrods: Experiments and numerical simulations. *Nanoscale* **7**, 7833–7840 (2015).
9. W. Duan, W. Wang, S. Das, V. Yadav, T. E. Mallouk, A. Sen, Synthetic nano- and micromachines in analytical chemistry: Sensing, migration, capture, delivery, and separation. *Annu. Rev. Anal. Chem.* **8**, 311–333 (2015).
10. A. B. Kersting, D. W. Efurd, D. L. Finnegan, D. J. Rokop, D. K. Smith, J. L. Thompson, Migration of plutonium in ground water at the Nevada Test Site. *Nature* **397**, 56–59 (1999).
11. T. K. Sen, K. C. Khilar, Review on subsurface colloids and colloid-associated contaminant transport in saturated porous media. *Adv. Colloid Interface Sci.* **119**, 71–96 (2006).
12. A. I. Abdel-Fattah, D. Zhou, H. Boukhalfa, S. Tarimala, S. D. Ware, A. A. Keller, Dispersion stability and electrokinetic properties of intrinsic plutonium colloids: Implications for subsurface transport. *Environ. Sci. Technol.* **47**, 5626–5634 (2013).
13. R. C. Goodknight, W. A. Klikoff Jr., I. Fatt, Non-steady-state fluid flow and diffusion in porous media containing dead-end pore volume. *J. Phys. Chem.* **64**, 1162–1168 (1960).
14. J. L. Anderson, Colloid transport by interfacial forces. *Annu. Rev. Fluid Mech.* **21**, 61–99 (1989).
15. V. G. Levich, V. S. Krylov, Surface-tension-driven phenomena. *Annu. Rev. Fluid Mech.* **1**, 293–316 (1969).
16. S. Marbach, L. Bocquet, Osmosis, from molecular insights to large-scale applications. *Chem. Soc. Rev.* **48**, 3102–3144 (2019).
17. R. W. O'Brien, L. R. White, Electrophoretic mobility of a spherical colloidal particle. *J. Chem. Soc. Faraday Trans. 2* **74**, 1607–1626 (1978).
18. Y. Hong, N. M. K. Blackman, N. D. Kopp, A. Sen, D. Velegol, Chemotaxis of nonbiological colloidal rods. *Phys. Rev. Lett.* **99**, 178103 (2007).
19. B. Abécassis, C. Cottin-Bizonne, C. Ybert, A. Ajdari, L. Bocquet, Boosting migration of large particles by solute contrasts. *Nat. Mater.* **7**, 785–789 (2008).
20. A. Kar, T.-Y. Chiang, I. Ortiz Rivera, A. Sen, D. Velegol, Enhanced transport into and out of dead-end pores. *ACS Nano* **9**, 746–753 (2015).
21. N. Singh, G. T. Vladisavljević, F. Nadal, C. Cottin-Bizonne, C. Pirat, G. Bolognesi, Reversible trapping of colloids in microgrooved channels via diffusiophoresis under steady-state solute gradients. *Phys. Rev. Lett.* **125**, 248002 (2020).
22. A. Banerjee, I. Williams, R. N. Azevedo, M. E. Helgeson, T. M. Squires, Soluto-inertial phenomena: Designing long-range, long-lasting, surface-specific interactions in suspensions. *Proc. Natl. Acad. Sci. U.S.A.* **113**, 8612–8617 (2016).
23. C. Jin, C. Krüger, C. C. Maass, Chemotaxis and autochemotaxis of self-propelling droplet swimmers. *Proc. Natl. Acad. Sci. U.S.A.* **114**, 5089–5094 (2017).
24. R. P. Sear, P. B. Warren, Diffusiophoresis in nonadsorbing polymer solutions: The Asakura-Oosawa model and stratification in drying films. *Phys. Rev. E* **96**, 062602 (2017).
25. X. Zhao, H. Palacci, V. Yadav, M. M. Spiering, M. K. Gilson, P. J. Butler, H. Hess, S. J. Benkovic, A. Sen, Substrate-driven chemotactic assembly in an enzyme cascade. *Nat. Chem.* **10**, 311–317 (2018).
26. A. Würger, Thermal non-equilibrium transport in colloids. *Rep. Prog. Phys.* **73**, 126601 (2010).
27. I. Lagzi, S. Soh, P. J. Wesson, K. P. Browne, B. A. Grzybowski, Maze solving by chemotactic droplets. *J. Am. Chem. Soc.* **132**, 1198–1199 (2010).
28. N. Shi, R. Nery-Azevedo, A. I. Abdel-Fattah, T. M. Squires, Diffusiophoretic focusing of suspended colloids. *Phys. Rev. Lett.* **117**, 258001 (2016).
29. S. Shin, O. Shardt, P. B. Warren, H. A. Stone, Membraneless water filtration using CO_2. *Nat. Commun.* **8**, 15181 (2017).
30. S. Shin, E. Um, B. Sabass, J. T. Ault, M. Rahimi, P. B. Warren, H. A. Stone, Size-dependent control of colloid transport via solute gradients in dead-end channels. *Proc. Natl. Acad. Sci. U.S.A.* **113**, 257–261 (2016).
31. N. O. Young, J. S. Goldstein, M. J. Block, The motion of bubbles in a vertical temperature gradient. *J. Fluid Mech.* **6**, 350–356 (1959).
32. Z. Lu, M. H. K. Schaarsberg, X. Zhu, L. Y. Yeo, D. Lohse, X. Zhang, Universal nanodroplet branches from confining the Ouzo effect. *Proc. Natl. Acad. Sci. U.S.A.* **114**, 10332–10337 (2017).
33. S. V. Hartman, B. Božič, J. Derganc, Migration of blood cells and phospholipid vesicles induced by concentration gradients in microcavities. *N. Biotechnol.* **47**, 60–66 (2018).
34. A. Banerjee, T. M. Squires, Long-range, selective, on-demand suspension interactions: Combining and triggering soluto-inertial beacons. *Sci. Adv.* **5**, eaax1893 (2019).
35. J. L. Anderson, D. C. Prieve, Diffusiophoresis: Migration of colloidal particles in gradients of solute concentration. *Sep. Purif. Technol.* **13**, 67–103 (1984).
36. B. V. Derjaguin, Y. I. Yalamov, A. I. Storozhilova, Diffusiophoresis of large aerosol particles. *J. Colloid Interface Sci.* **22**, 117–125 (1966).
37. D. Lohse, X. Zhang, Physicochemical hydrodynamics of droplets out of equilibrium. *Nat. Rev. Phys.* **2**, 426–443 (2020).
38. C. J. Wienken, P. Baaske, U. Rothbauer, D. Braun, S. Duhr, Protein-binding assays in biological liquids using microscale thermophoresis. *Nat. Commun.* **1**, 100 (2010).
39. H. Manikantan, T. M. Squires, Surfactant dynamics: Hidden variables controlling fluid flows. *J. Fluid Mech.* **892**, P1 (2020).
40. V. G. Levich, A. M. Kuznetsov, Motion of drops in liquids under the influence of surface-active substances. *Dokl. Akad. Nauk SSSR* **146**, 145–147 (1962).
41. K. C. Tam, E. Wyn-Jones, Insights on polymer surfactant complex structures during the binding of surfactants to polymers as measured by equilibrium and structural techniques. *Chem. Soc. Rev.* **35**, 693–709 (2006).
42. A. G. Kanellopoulos, M. J. Owen, Adsorption of sodium dodecyl sulphate at the silicone fluid/water interface. *Trans. Faraday Soc.* **67**, 3127–3138 (1971).
43. M. H. Abraham, H. S. Chadha, G. S. Whiting, R. C. Mitchell, Hydrogen bonding. 32. An analysis of water-octanol and water-alkane partitioning and the Δlog p parameter of Seiler. *J. Pharm. Sci.* **83**, 1085–1100 (1994).
44. C. Erkey, K. A. Alhamid, A. Akgerman, Investigation of the effects of molecular association on diffusion in binary liquid mixtures at the infinite dilution limit. *J. Chem. Phys.* **94**, 3867–3871 (1991).
45. S. Shin, V. S. Doan, J. Feng, Osmotic delivery and release of lipid-encapsulated molecules via sequential solution exchange. *Phys. Rev. Appl.* **12**, 024014 (2019).
46. D. Velegol, A. Garg, R. Guha, A. Kar, M. Kumar, Origins of concentration gradients for diffusiophoresis. *Soft Matter* **12**, 4686–4703 (2016).
47. D. Bartolo, G. Degré, P. Nghe, V. Studer, Microfluidic stickers. *Lab Chip* **8**, 274–279 (2008).
48. L.-H. Hung, R. Lin, A. P. Lee, Rapid microfabrication of solvent-resistant biocompatible microfluidic devices. *Lab Chip* **8**, 983–987 (2008).
49. J. S. Paustian, R. N. Azevedo, S.-T. B. Lundin, M. J. Gilkey, T. M. Squires, Microfluidic microdialysis: Spatiotemporal control over solution microenvironments using integrated hydrogel membrane microwindows. *Phys. Rev. X* **3**, 041010 (2013).

Acknowledgments

Funding: We acknowledge the funding support from the Saudi Arabian Oil Company (Saudi Aramco Contract A-0002-2018) and the joint collaboration with Saudi Aramco EXPEC ARC's Upstream Nanotechnology team. A portion of this work was performed in the Microfluidics Laboratory within the California NanoSystems Institute, supported by the University of California, Santa Barbara and the University of California, Office of the President, and in the shared facilities of the UCSB MRSEC (NSF DMR 1720256), a member of the Materials

Research Facilities Network. **Author contributions:** H.T. and T.M.S. designed the research. H.T. fabricated the devices with input from A.B. and N.S. H.T. performed experiments and analyzed the data. H.T. performed simulations. H.T. and T.M.S. built the model. H.T., X.T., A.A.-F., and T.M.S. discussed the results. H.T. and T.M.S. wrote the paper, and A.A.-F., H.T., and T.M.S. revised the paper. **Competing interests:** H.T. and T.M.S. are inventors on a patent application relating to the strategy described in this work. All other authors declare that they have no competing interests. **Data and materials availability:** All data needed to evaluate the conclusions in the paper are present in the paper and/or the Supplementary Materials.

Submitted 15 February 2021
Accepted 25 June 2021
Published 13 August 2021
10.1126/sciadv.abh0638

Citation: H. Tan, A. Banerjee, N. Shi, X. Tang, A. Abdel-Fattah, T. M. Squires, A two-step strategy for delivering particles to targets hidden within microfabricated porous media. *Sci. Adv.* **7**, eabh0638 (2021).